PHOTONICS Research

Doppler velocimeter based on dual-comb absorption spectroscopy

Chenglin Gu,† Xing Zou,† Zhong Zuo, Daowang Peng, Yuanfeng Di, Yang Liu, Daping Luo, and Wenxue Li*

State Key Laboratory of Precision Spectroscopy, East China Normal University, Shanghai 200062, China
**Corresponding author: wxli@phy.ecnu.edu.cn*

Received 3 August 2020; revised 23 September 2020; accepted 8 October 2020; posted 12 October 2020 (Doc. ID 398876); published 23 November 2020

The determination of airflow parameters is essential to the research of critical information on environment monitoring, chemical kinetics, and aerodynamic and propulsion applications. During the past few decades, tunable diode laser absorption spectroscopy has become a common and efficient tool for the flow velocity measurement based on the Doppler shift of the absorption line. Dual-comb absorption spectroscopy (DCAS), as a state-of-the-art Fourier-transform broadband spectroscopic technique, not only can detect multiple trace molecules in parallel but also can extract Doppler shifts to derive the flow velocity through the analysis of dozens of molecular absorption lines simultaneously with high precision. Here, we report a proof-of-principle demonstration of the velocity measurements of acetylene at various flow velocities by means of a high-resolution and broadband DCAS. Mode-resolved Doppler-shifted rotational-vibrational lines in the P branch of acetylene molecules are obtained. A model for multiline Doppler frequency determination is investigated and experimentally verified. The flow velocity measurements with a measuring uncertainty down to the submeter per second over the range from 8.7 m/s to 44.8 m/s at an effective time resolution of 1 s and a measuring uncertainty of 1.97 m/s at 0.1 s are demonstrated. With broadband mid-infrared frequency combs covering atmospheric transmission windows, the open-path measurement for monitoring diffusion of the weak pollutant source would be realized.

https://doi.org/10.1364/PRJ.398876

1. INTRODUCTION

As an important application of optical frequency combs (OFCs), dual-comb absorption spectroscopy (DCAS) uses two phase-locked combs with a slightly different repetition to one-to-one map the amplitude and phase information of the comb teeth from the optical domain to the RF domain on a single photodetector [1,2]. It has been demonstrated to be a powerful tool in various scientific fields for time-resolved, broadband, and high-resolution spectroscopic measurements with excellent sensitivity [3–9]. In particular, a series of remarkable works about the sensitive detection of trace gas molecules and the open-path atmospheric monitoring with frequency comb spectroscopy already has made dramatic progress [10–16]. Meanwhile, it is an urgent demand for the parallel sensing of multiple dynamic trace molecules, such as the leakage and diffusion process of pollutants, to realize the sensitive detection of gas molecules and the determination of the flow direction of molecules simultaneously.

Besides the dynamic trace pollutants, the capability of experimentally determining the flow velocity is beneficial to the study of scientific fields, such as the prediction of physical mechanisms, aerodynamic systems, weather forecasting, and biomedical engineering [17–22]. Among all solutions for the flow velocity measurement, the optical velocimeter stands out due to its rapid and nonintrusive nature [23] and has been playing an important role in various applications since its invention. By using the laser-induced fluorescence velocity measurement, a series of flow visualizations in high-speed compressible flows with the velocity up to 4060 m/s was performed, and the accuracies of a few percent of the maximum velocity at an effective acquisition rate of 10 Hz were obtained [24,25]. However, the absolute concentration of exhaust emissions cannot be measured, and the addition of seed molecules may be harmful to sensitive ground test facilities. Furthermore, a nonlinear optical method such as coherent anti-Stokes Raman scattering (CARS), with the advantages of spectral selectivity and laser-like directional signal was applied in a velocity measurement for the low-enthalpy wind tunnels. With this velocimeter, the laminar flow for the expected velocity of 1382 m/s can be measured with the accuracy of 6% [26], but it may suffer from the low intensity level of the CARS signal, limiting the acquisition time to 40 s [27]. For the range-resolved wind detection in

the low-speed airflow, the velocimeter using the molecular scattering has been proved to be an effective instrument within the velocity sensitivity of 5% at the temporal resolution of seconds, but the necessity of the laser pulse with high energy hinders its further wide application [28,29]. Tunable diode laser absorption spectroscopy (TDLAS) for the flow velocity measurement offers the practical advantages of robustness and sensitivity, and besides that, velocity, temperature, pressure, and mass flux can also be inferred from details of the absorption lines [30,31]. Combining TDLAS with the wavelength modulation spectroscopy with $2f$ detection, the time-resolved velocity measurements for the practical applications ranging from the low-speed wind tunnel to advanced aero-propulsion devices were achieved within the uncertainty of 1% due to superior noise rejection capabilities [32–34]. However, to recover the complete absorption line, TDLAS usually requires the repetitive wavelength scanning and one etalon signal as the frequency marker to provide a fine calibration of the wavenumber axis of the absorption spectrum simultaneously [35].

Benefiting from the broadband and extremely precise spectroscopic performance of the DCAS, the airflow velocity measurement based on the DCAS has several advantages. (1) Through the analysis of Doppler shifts of absorption lines, not only does DCAS have the capacity of distinguishing multiple unknown gas molecules sensitively but also can determine the flow direction of molecules simultaneously. This is significant for research on leakage and diffusion process of pollutants in the wind flow. (2) A broadband spectrum in a single measurement enables parallel measurement of hundreds of molecular absorption lines simultaneously, which improves the precision of Doppler-shifted frequency measurements [36,37]. Furthermore, parallel sensing of gas molecules with broadband OFCs [38] is able to select series of spectral regions that minimize the interference from ambient interfering molecules, thus eliminating the risk from overlapped absorption lines. (3) Using the heterodyne detection of two combs with slightly different repetition frequencies, DCAS gets rid of scanning processes and obtains the periodic interferograms with a period of milli- or microseconds, allowing for time-resolved spectroscopy [39]. The comb requires no additional calibration and can be either phase-locked to the ultrastable RF reference through f–$2f$ self-referencing technique [40] or referenced to a stable narrow linewidth laser [41]. (4) DCAS, as a Fourier transform spectrometer, inherits the Fellgett's advantage over an equivalent scanning monochromator because all spectral information is measured simultaneously on a single photodetector. This basically results in the consistency of the measurement and a relative improvement in the detector noise limit. Moreover, the heterodyne detection characteristic of DCAS in the RF spectrum (10s–100s of megahertz) can effectively reduce the $1/f$ noise.

In the experiments, we present a comb-mode-resolved dual-comb spectrum to extract the Doppler shift frequency, which covers the P branch of a C_2H_2 molecule ranging from 193.4 to 196.6 THz. The signal-to-noise ratio (SNR) of multiple absorption lines is obtained, and its impact on the statistical uncertainty of the line center fitting is discussed, which turns out to be consistent with experimental results. We also introduce the weighted average model for the unequal-uncertainty measurements to optimize the measuring uncertainty. The velocities of acetylene ranging from 8.72 m/s to 44.87 m/s with an uncertainty down to 0.19 m/s are obtained within a 15 s measurement time. Through the implementation of a time-dependent dynamic monitoring of various flow velocities with an invariant measuring uncertainty (~0.6 m/s, that is, 1.5% of the maximum velocity) at the effective time resolution of 1 s throughout, the potential applications of the DCAS velocimeter in the diagnostics of propulsion system and pollutant diffusion in the wind flow are demonstrated.

2. EXPERIMENTAL SCHEMATIC AND SETUP

Figure 1(a) presents the concept of our DCAS-based velocimetry system. When the laser beam propagates forward in a cell, multiple absorption line centers of the moving gaseous molecule are Doppler-shifted up in frequency. Conventionally, accurate quantification of frequency shifts is achieved through assessing the centers of absorption line profiles in DCAS, which is given by $\Delta f_D = f_0(V/c)\cos\vartheta$, where V is the airflow velocity, c is the speed of light, f_0 is the line-center frequency, and ϑ is the angle between the velocity vector and the optical axis. We propose a counterpropagating collinear laser beam arrangement to cancel the residual frequency drift and allow the flow velocity to be derived from the absorption peak pairs in both blue and red Doppler-shifted spectra. Since the flow velocities are obtained from dozens of parallel shifted lines in the

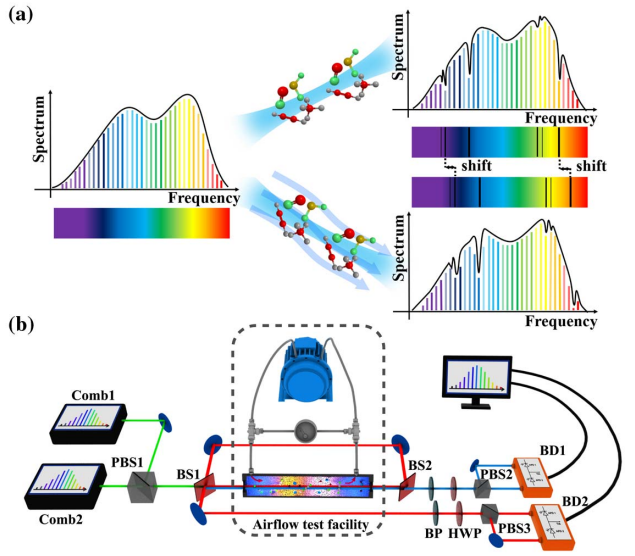

Fig. 1. Schematic and experimental layout for the gas flow velocity measurements based on DCAS. (a) Multiple absorption lines experience Doppler shifts in the line-center frequency. DCAS enables the extraction of the precise position of each absorption line center, and the flow velocity can be derived from frequency shifts of multiple absorption lines. (b) The outputs of two combs are combined and split into two subbeams for the counterpropagating arrangement. The airflow is produced in the test facility by a commercially vacuum pump. PBS, polarization beam splitter; BS, beam splitter; BP, bandpass filter; HWP, half-wave plate; BD, balanced detector.

broadband spectrum, our measuring uncertainty is improved compared to single-peak measurements.

Figure 1(b) presents the configuration of our DCAS-based velocimetry system, and the generation of the passive mutually coherent dual-comb spectrometer is based on our previous work using the ultrafast optical modulation technique [42]. The optical sources are two frequency combs with comb repetition rates of 108 MHz that differ by $\Delta f_r = 1.2$ kHz. Two combs have 3 THz spectral bandwidths to cover 193.4 to 196.6 THz (1550–1525 nm). It means that the combs consist of 30,000 frequency modes, which is equivalent to the output of the same amount of narrow linewidth continuous wave (CW) frequency components. Then, two combs are combined spatially on a polarization beam splitter and transmitted through the sample together, which achieves a symmetric approach. Such an approach overcomes random variations of the laser phase when the system is subject to turbulent or chaotic environments [2,43]. It is worth mentioning that a 50:50 beam splitter is utilized to split the combined beams to obtain two counterpropagating measuring beams. This not only eliminates the residual frequency drift of combs but also receives twice the magnitude of the Doppler shift between the respective blue- and redshifted frequency signals. The counterpropagating beams are spatially offset with a slight angle of 1 deg. As such, both beams are separate when the detector is far from the beam splitter. The flow velocity measurements are performed in an airflow test facility. The gas cell is a 40-cm long cylindrical tube with a diameter of 4 mm. The small diameter can obtain a relative high flow velocity with the same air-pump power. A pair of quartz plates with wedge angles of 3 deg located at both ends of the tube serves as optical windows. The air-pump equipment is a commercially available, 250 L/min exhaust-flow vacuum pump (ISP-250c from ANEST IWATA). The airflow is produced at whole circular pipelines once a parallel connection is established between the cell and pump, and the airflow velocity is controlled by an adjustable split-flow component. After the gas-flowing cell, we use an optical bandpass filter to optimize the spectral region to meet Nyquist sampling conditions, thereby avoiding the aliasing effects. Certainly, ultrabroadband lasers such as supercontinuum sources have the potential to realize parallel gas sensing and velocity measurements simultaneously [44]. A half-wave plate and a polarizing beam splitter are used to fine-tune the balancing of light levels. Then, the two comb lasers with the same power levels are guided to two ports of a 150 MHz commercial balanced detector (PDB450 C from Thorlabs) for the heterodyne spectral signal detection. To avoid the nonlinearity or full saturation of the detector that could lead to slight distortions of the measured absorption line centers, the total average power of the two combs into each port of the detector is attenuated to ~0.5 mW. A low-pass filter at 48 MHz is applied to the electronic signals to avoid aliasing of signals. The detector signals are then digitized by a 160 MS/s 16-bit data-acquisition board (ATS9462 from AlazarTech). In this experiment, the adaptive sampling technique is adopted to eliminate the residual drift of the repetition frequency difference between two combs. The streams of recorded raw data are then directly fast Fourier-transformed to achieve the dual-comb spectrum.

3. RESULTS AND DISCUSSIONS

To evaluate the performance of our dual-comb spectroscopy, we measure a mode-resolved spectrum of static acetylene at a pressure of 5 mbar. Streams of data containing series of interferograms spaced by $1/\Delta f_r = 833$ μs are recorded within a time window of up to 10 s. The spectrum of the raw data is obtained by the fast Fourier transform (FFT) and is shown in Fig. 2(a). For the measurement time of 10 s, the SNR culminates at 421 around 6470 cm^{-1}, and the average SNR across the entire span of 3.2 THz is 198. The resulting figure of merit (SNR × M at 1-s averaging time), calculated for the average SNR, is therefore 1.88×10^6 $Hz^{1/2}$, where M is the number of comb lines across the optical bandwidth. Figure 2(b) is a zoomed view of the spectrum, which clearly shows the discrete comb line intensities shaped by C_2H_2 absorption profiles. Our optical sampling f_r is ~108 MHz (stabilized to the Rb frequency standard) and is essential especially for highly crowded spectral features at low pressure, such as a P branch composed of Doppler-broadened lines. Moreover, for our homemade frequency combs, this spacing is easy to adjust to match the requested spectral resolution. The full width at half-maximum (FWHM) of the RF comb lines is 100 MHz (9 kHz in the optical scale), which equals to the Fourier-transform limit of the 10 s-long recording time. In this experiment, our DCAS is passively phase-locked to the narrow linewidth CW laser (Koheras Adjust E15, NKT Photonics, with a claimed free-running linewidth of less than 0.1 kHz at a 100 μs integration time). Although there is a long-term frequency shift resulting from the drift of the commercial CW reference laser of roughly 1 MHz/min, the concern of the DCAS-based Doppler velocimeter is the Doppler-shifted frequency between two counterpropagating laser beams, which can effectively eliminate the residual frequency drift from the CW laser. In principle, when the combs are referenced to a frequency standard by means of f–$2f$ self-referencing technique [45] (which is not adopted in this experiment) the long-term frequency shift can all be removed, enabling the unidirectional measurements with a high precision. As presented in Fig. 2(c), the retrieved dual-comb spectrum is highly consistent with the transmission spectrum computed from the HITRAN database. Multiple rovibrational lines in the half of the P branch of C_2H_2 are clearly identified, which enables multiple flow velocity measurements in a single spectrum measurement simultaneously.

As in the traditional TDLAS velocimeter, determining the line centers of the absorption profiles for a DCAS velocimeter is also crucial. DCAS takes advantage of the parallel recording of multiple absorption lines and realizes flow velocity measurements with multiline analysis. Figure 3 shows the measured absorption spectra retrieved from counterpropagating beams and several blue- and red-shifted absorption peak pairs in 1 s recording time. The FWHM of the absorption line $\Delta\nu_{\mathrm{FWHM}}$ varies from 720 to 1200 MHz due to the combined effect of Doppler- and collision-broadening in the airflow. A higher sampling rate can result in a better line fitting, and thus more precise line-center identification. As such, we use the zero-padding approach to achieve fine interpolation line shapes in the frequency spectrum [46]. Then, the profiles near the peak of rovibrational lines are least-squares fitted by a

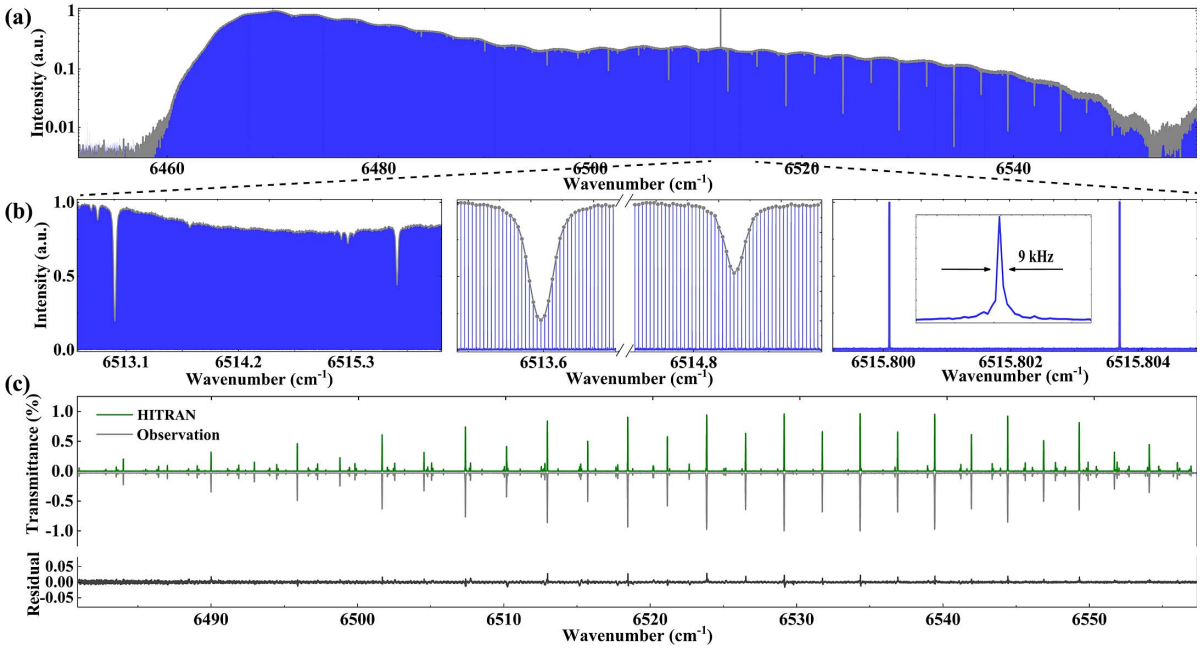

Fig. 2. Comb-mode-resolved DCAS. (a) Broadband optical spectrum (log scale) obtained via FFT from a 10-s-long recording. (b) Zoomed figures display comb-tooth-resolved spectra with absorbed energy modes resulting from C_2H_2 absorption. The comb-mode spectrum is resolved with an optical sampling of 108 MHz. The inset shows an individual comb tooth with a linewidth of 9 kHz in the optical scale. (c) Experimental absorption spectrum (gray curve) of static acetylene with 5 mbar is compared with a spectrum (green curve) computed from the same parameters in the HITRAN database, along with the residuals.

Lorentzian distribution function using a nonlinear Levenberg–Marquardt algorithm. We observe that there is little difference between the Lorentzian and Voigt line shapes for the fitting of the data points near the peak. The precise position of each absorption line center is obtained through the least-squares fitting routine. Flow velocity is obtained by calculating the Doppler shifts between multiple blue- and red-shifted line pairs across the measured bandwidth.

For the Doppler velocimeter, the flow velocity is derived from the determination of the line centers between the Doppler shift absorption profiles. Therefore, the uncertainty of the optical velocity measurement mainly depends on two factors: the stability of the laser source, and the uncertainty of the data acquired. The stability of the frequency comb has been demonstrated in series of works [47,48]. The error in our experiment is mainly due to the line-shape fitting process used for extracting the Doppler shift frequency. One concern is the limited SNR of our DCAS due to the presence of the noise (as in all laser spectrometers) and its influence on the line-center determination [49]. In theory, the statistical uncertainty on the ith fitting line center for the Lorentzian fitting is [50]

$$\delta_i = \frac{2 \times \Delta v_{\mathrm{FWHM}}}{\mathrm{SNR}_i \times \sqrt{N_{\mathrm{pnts}}}}, \tag{1}$$

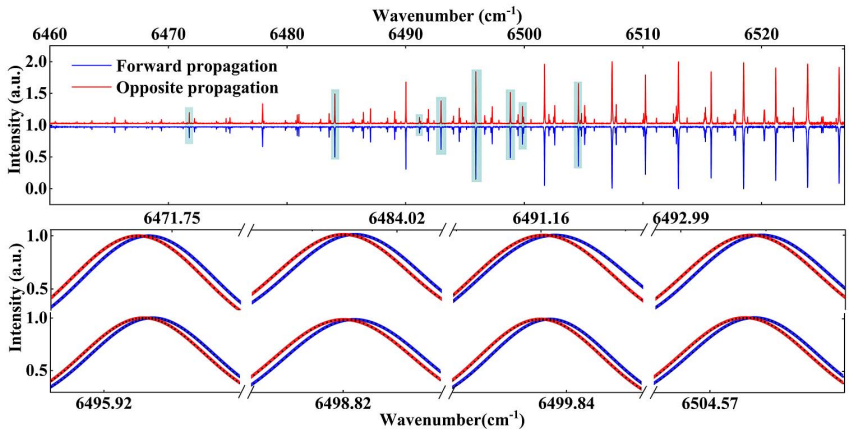

Fig. 3. Absorption spectra of the acetylene flow at a pressure of 15 mbar from forward (blue curve) and opposite (red curve) measurements in 1 s recording time. Doppler-shifted absorption peak pairs in cyan-shaded boxes are shown in the zooms below.

where SNR_i is the SNR of the ith peak, $N_{\mathrm{pnts}} = \Delta v_{\mathrm{FWHM}}/f_r$ is the number of measured points across the FWHM; SNR_i equals to I_i/σ, I_i is the absorption spectral intensity at the center of the absorption line, and σ is the standard deviation of the noise. The statistical uncertainty on the fitting line center can be experimentally validated. Since δ_i is mainly determined by SNR, the Doppler-shifted peak pairs with close SNR can be treated as individual independent measurements with a similar standard deviation. Therefore, the standard deviation of a single absorption line can be extracted from multiple absorption lines with close SNRs in a single measurement. To confirm the theoretical prediction, we take the standard deviation of the measured velocities derived from 10 Doppler-shifted peak pairs with close SNR range, and compare it against the predictive uncertainty of an individual absorption line with an average SNR of the range using Eq. (1). The selected absorption lines from the dual-comb spectrum in various measurement times are extracted, as shown in Fig. 4. As an example, the standard deviation of the measured velocities is 3.59 m/s in 1 s measurement time for absorption lines, with the SNR ranging from 100 to 250. The theoretical statistical uncertainty is calculated to be 4.68 m/s ($\sim 3.31 \times \sqrt{2}$ due to the counterpropagating arrangement) based on Eq. (1) for an absorption line with the average SNR of 175. The consistency between the theoretical uncertainties and the experimental results in different recording times in Fig. 4 proves that the measuring uncertainty of an individual absorption peak can be evaluated effectively with the statistical uncertainty based on Eq. (1).

DCAS is capable of sensing dozens of Doppler-shifted absorption lines and achieves a superior measuring uncertainty over single-peak measurements. Since the statistical uncertainty δ_i is inversely proportional to SNR_i of the ith peak, multiple peaks with different SNR_i in a single spectrum can be treated as an unequal-uncertainty measurement. We thereby introduce

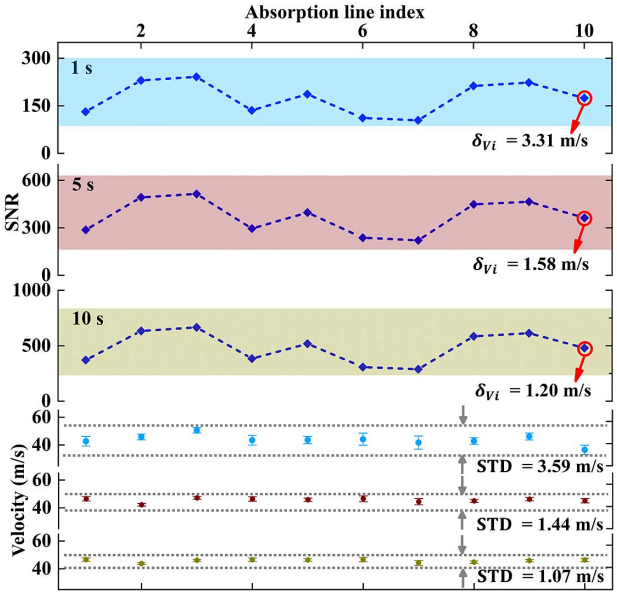

Fig. 4. Comparison between the theoretical uncertainty δ_{Vi} and the standard deviation (STD) of the measured velocities in different measurement times (the curves from top to bottom corresponding to 1, 5, and 10 s, respectively).

weighted average to obtain the optimal measuring uncertainty for the unequal-uncertainty measurement. The weight of the ith peak is

$$P_i = \frac{\delta_{\min}^2}{\delta_i^2}, \tag{2}$$

where the absorption line with highest SNR (i.e., the statistical uncertainty $\delta_{\min}$) is defined as the unit weight. Accordingly, the weighted-averaging flow velocity can be expressed as

$$\overline{V} = \sum \left(\frac{P_i}{\sum P_i} V_i \right), \tag{3}$$

where V_i is the measured flow velocity inferred from the frequency shift of the ith absorption peak pairs, and the corresponding measuring uncertainty is

$$\delta_{\overline{V}} = \frac{\delta_{V\min}}{\sqrt{\sum P_i}}, \tag{4}$$

where $\delta_{V\min}$ is the multiplication of the unit weight $\delta_{\min}$ and a coefficient from the Doppler effect. Figure 5(a) shows flow velocities derived from dozens of absorption lines within our spectral coverage and their corresponding SNRs at different measurement times. According to our calculation, the flow velocity is 46.73 m/s with the measuring uncertainty of 1.97 m/s in 0.1 s according to Eq. (4), and 45.73 m/s with the uncertainty of 0.19 m/s in 15 s. It is obvious that the uncertainty of the velocity is improved with time due to the signal averaging effect not only in DCAS but also in other optical velocimeters such as TDLAS. The optimum averaging time is related to the stable time that the measurement system can keep. For TDLAS, the optimum averaging time is typically dozens of seconds [51], while for DCAS, a coherent averaging time of 1860 s has already been demonstrated, which has the potential to be further increased [52]. Figure 5(b) shows the evolution of the measuring uncertainty with averaging time. The measuring uncertainty decreases with the square root of the measurement time due to the high stability of comb sources. An averaging time of 200 s with a measuring uncertainty of 0.059 m/s is achieved, and the trend has not reached the limitation of our system. It should be noted that even though the velocity measurement rarely takes hundreds of seconds (typically 0.1 to 10 s), a continuous velocity monitor will benefit from the long-time stability.

An important factor to assess the noise characteristics of the different types of spectroscopic instruments is the figure of merit (quality factor) because it takes into account both the spectral coverage and the SNR. In case the laser relative intensity noise is suppressed to a relatively low level, the DCAS and the TDLAS both have the same level of figure of merit when the same optical sensing configuration and detection elements are used. However, the SNR of the TDLAS is higher than that of the former, generally due to the narrow bandwidth of the TDLAS. According to the basic scaling law of the figure of merit, it illustrates the trade-off between the average SNR and the number of comb lines across the optical bandwidth [53]. In principle, the SNR of the DCAS can be increased up to the level of the TDLAS when the measured bandwidth is decreased to that of the latter if a high-precision velocity measurement is required.

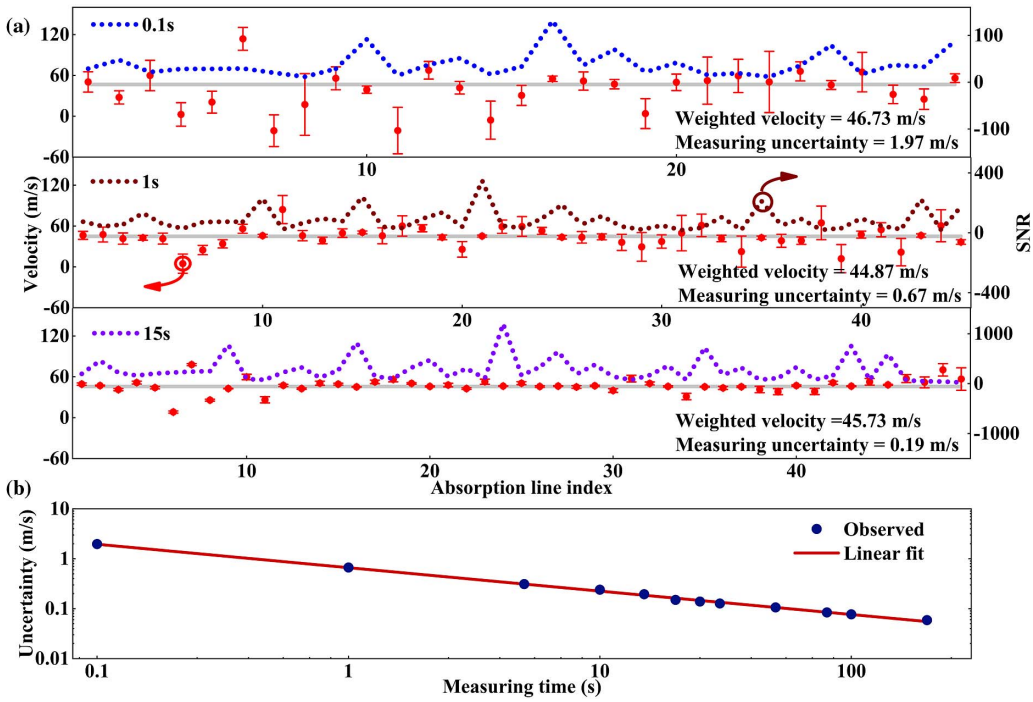

Fig. 5. Gas flow velocity measurements with DCAS. (a) Experimental flow velocities (red dots) are derived from Doppler shifts of dozens of absorption lines. The SNR (the dotted-line from top to bottom corresponding to 0.1, 1, and 15 s measurement time, respectively) of each absorption line is applied to Eq. (1), and then extracted to calculate the statistical uncertainty at the fitting line center. The increasing number of available absorption lines is attributed to undistorted absorption lines with the signal averaging. The weighted-average flow velocities (gray curve) with different measuring uncertainties are obtained. (b) Evolution of the measuring uncertainty with the acquisition time. A linear fit with a slope of 0.469 indicates that the measuring uncertainty is inversely proportional to the square root of the measurement time.

The measuring uncertainty of the DCAS velocimeter can be further validated experimentally by the measured velocity when the airflow is static (the velocity is zero). In this static condition, Fig. 6(a) shows several measured absorption peak pairs retrieved from counterpropagating beams in 1 s measurement time. Figure 6(b) shows the measured flow velocities from multiple absorption peak pairs with different SNRs. According to the model of weighted average for the multiple absorption lines, the flow velocity in the static gas is 0.38 m/s with a measuring uncertainty of 0.72 m/s in 1 s measurement time, and −0.02 m/s with an uncertainty of 0.21 m/s in 15 s. The results for the measured velocities (0.38 and −0.02 m/s) within the range of the measuring uncertainties (0.72 and 0.21 m/s) in different recording times demonstrate the validity of the measuring uncertainty based on Eq. (4). For practical applications such as combustion chambers, the molecules of carbon dioxide and water vapor, CO_2 and H_2O, tend to be the key species for tracing the diffusion velocity of the airflow field. Note that

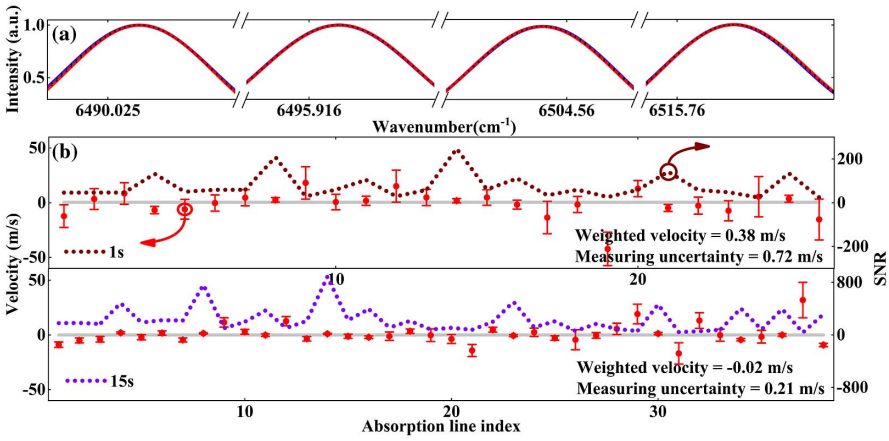

Fig. 6. Velocity measurements of static gas with DCAS. (a) Absorption peak pairs in 1 s measurement time; (b) measured flow velocities (red dot) and the SNR (brown and purple dotted lines corresponding to 1 s and 15 s recording times) extracted from multiple absorption peak pairs.

most molecules in the gas phase have relatively strong rovibrational transitions in the mid-infrared spectral range. The effective improvement of the DCAS sensitivity with mid-infrared frequency combs can be proposed as the solution.

Experiments for various flow velocity measurements are also carried out by the DCAS velocimeter. The Doppler shift varies within the range from 11.33 to 58.29 MHz, as shown in Fig. 7(a). The measured maximum and minimum flow velocities are 44.87 and 8.72 m/s, respectively, when the valves in the test facility are fully closed and opened. The Doppler-shifted peak pairs in Fig. 7(b) show the increasing frequency shift with the flow velocity. It is worth noting that all measured flow velocities still maintain similar measuring uncertainty (~0.6 m/s) in 1 s time resolution at various flow velocities throughout. The minimum measuring uncertainty for flow determination is 1.5% within 1 s, and this is expected to decrease as the flow velocity increases. As such, the DCAS velocimeter has the potential to perform a high-precision measurement for high-speed applications such as hypersonic wind tunnels.

Figure 8 shows a continuous dynamic monitoring of the flow velocity in 40 s by the DCAS velocimeter. The test facility is stepped up to successively higher velocities at 8.72, 20.00, 30.43, and 44.87 m/s through the control of the valve in a 10 s time interval. The recorded data are provided at an effective time resolution of 1 s without postprocessing and reach a measuring uncertainty of submeter per second. The velocity fluctuations of less than 2 m/s can be observed in the zoomed plots in Fig. 8. The fluctuation is mainly due to the unsteady exhaust flow of the vacuum pump and the turbulent flow in the test facility.

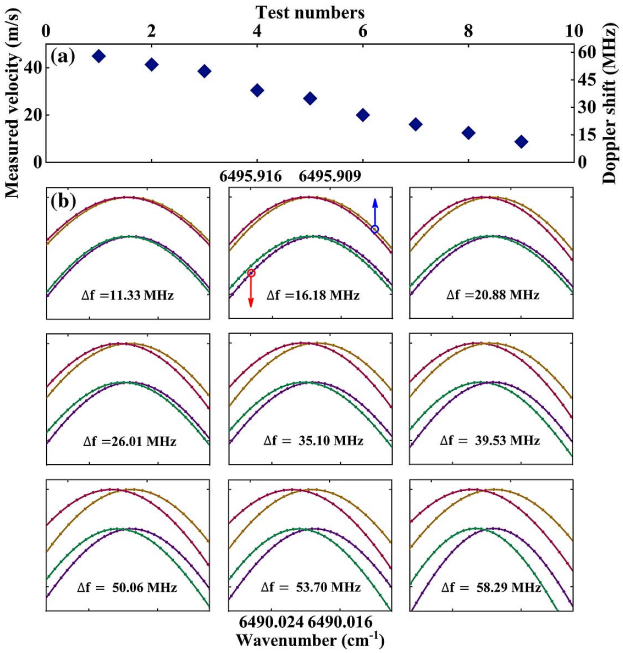

Fig. 7. Experiments for various flow velocities with DCAS. (a) Flow velocity measurements with DCAS in the range from 8.72 to 44.87 m/s; (b) two selected absorption line pairs with forward (red and green curves) and opposite (yellow and purple curves) Doppler shifts in an acquisition time of 1 s at different flow velocities. The Doppler shift varies from 11.33 to 58.29 MHz with the velocity.

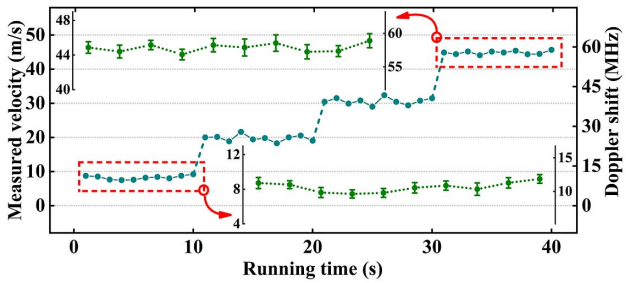

Fig. 8. Dynamic monitoring at 1 Hz over 40 s in the airflow test facility. The measured flow velocity is stepped up in a 10 s time interval. A velocity fluctuation caused by unsteady exhaust-flow ~2 m/s is observed with the measuring uncertainty of 0.67 m/s.

4. CONCLUSION

In conclusion, we have developed and experimentally validated accurate velocity measurements in the airflow test facility with the DCAS velocimeter. In this pilot demonstration, a measuring uncertainty down to submeter per second at various flow velocities is achieved when the multiple absorption lines are processed with the weighted average model. This solution has the potential capability for low- and high-speed environmental applications such as pollutant diffusion, boundary-layer profiling, and hazardous plume and combustion systems. In addition, the performance of the DCAS velocimeter promises to be further improved by broadband OFCs in the mid-infrared region reported by several groups [54–57], where the stronger and highly crowded spectral lines are addressed. Going forward, utilizing the wavelength division configuration in multidimension based on the broadband DCAS, quantitative visualization of the flow field would be possible with a single photodetector.

Funding. National Natural Science Foundation of China (11874153, 11904105); National Key Research and Development Program of China (2018YFA0306301).

Disclosures. The authors declare no conflicts of interest.

†These authors contributed equally to this work.

REFERENCES

1. N. Picqué and T. W. Hänsch, "Frequency comb spectroscopy," Nat. Photonics **13**, 146–157 (2019).
2. I. Coddington, N. Newbury, and W. Swann, "Dual-comb spectroscopy," Optica **3**, 414–426 (2016).
3. P. Martín-Mateos, F. U. Khan, and O. E. Bonilla-Manrique, "Direct hyperspectral dual-comb imaging," Optica **7**, 199–202 (2020).
4. J. Bergevin, T. Wu, J. Yeak, B. E. Brumfield, S. S. Harilal, M. C. Phillips, and R. J. Jones, "Dual-comb spectroscopy of laser-induced plasmas," Nat. Commun. **9**, 1273 (2018).
5. T. Minamikawa, Y. Hsieh, K. Shibuya, E. Hase, Y. Kaneoka, S. Okubo, H. Inaba, Y. Mizutani, H. Yamamoto, T. Iwata, and T. Yasui, "Dual-comb spectroscopic ellipsometry," Nat. Commun. **8**, 610 (2017).
6. M. Suh, Q. Yang, K. Y. Yang, X. Yi, and K. J. Vahala, "Microresonator soliton dual-comb spectroscopy," Science **354**, 600–603 (2016).

7. N. H. Pinkowski, Y. Ding, C. L. Strand, R. K. Hanson, R. Horvarth, and M. Geiser, "Dual-comb spectroscopy for high-temperature reaction kinetics," Meas. Sci. Technol. **31**, 055501 (2020).
8. P. J. Schroeder, R. J. Wright, S. Coburn, B. Sodergren, K. C. Cossel, S. Droste, G. W. Truong, E. Baumann, F. R. Giorgetta, I. Coddington, N. R. Newbury, and G. B. Rieker, "Dual frequency comb laser absorption spectroscopy in a 16 MW gas turbine exhaust," Proc. Combust. Inst. **36**, 4565–4573 (2017).
9. A. D. Draper, R. K. Cole, A. S. Makowiecki, J. Mohr, A. Zdanowicz, A. Marchese, N. Hoghooghi, and G. B. Rieker, "Broadband dual-frequency comb spectroscopy in a rapid compression machine," Opt. Express **27**, 10814–10825 (2019).
10. T. Ideguchi, A. Poisson, G. Guelachvili, N. Picqué, and T. W. Hänsch, "Adaptive real-time dual-comb spectroscopy," Nat. Commun. **5**, 3375 (2014).
11. G. Millot, S. Pitois, M. Yan, T. Hovhannisyan, A. Bendahmane, T. W. Hänsch, and N. Picqué, "Frequency-agile dual-comb spectroscopy," Nat. Photonics **10**, 27–30 (2016).
12. K. C. Cossel, E. M. Waxman, F. R. Giorgetta, M. Cermak, I. R. Coddington, D. Hesselius, S. Ruben, W. C. Swann, G. Truong, G. B. Rieker, and N. R. Newbury, "Open-path dual-comb spectroscopy to an airborne retroreflector," Optica **4**, 724–728 (2017).
13. G. Ycas, F. R. Giorgetta, K. C. Cossel, E. M. Waxman, E. Baumann, N. R. Newbury, and I. Coddington, "Mid-infrared dual-comb spectroscopy of volatile organic compounds across long open-air paths," Optica **6**, 165–168 (2019).
14. T. Ideguchi, A. Poisson, G. Guelachvili, T. W. Hänsch, and N. Picqué, "Adaptive dual-comb spectroscopy in the green region," Opt. Lett. **37**, 4847–4849 (2012).
15. J. Mandon, G. Guelachvili, and N. Picqué, "Fourier transform spectroscopy with a laser frequency comb," Nat. Photonics **3**, 99–102 (2009).
16. E. Sorokin, I. T. Sorokina, J. Mandon, G. Guelachvili, and N. Picqué, "Sensitive multiplex spectroscopy in the molecular fingerprint 2.4 μm region with a Cr^{2+}:ZnSe femtosecond laser," Opt. Lett. **15**, 16540–16545 (2007).
17. T. S. Strickler, T. K. Langin, P. McQuillen, J. Daligault, and T. C. Killian, "Experimental measurement of self-diffusion in a strongly coupled plasma," Phys. Rev. X **6**, 021021 (2016).
18. F. Zhao and H. Hiroyasu, "The applications of laser Rayleigh scattering to combustion diagnostics," Proc. Combust. Inst. **19**, 447–485 (1993).
19. E. W. Rothe and P. Andresen, "Application of tunable excimer lasers to combustion diagnostics: a review," Appl. Opt. **36**, 3971–4033 (1997).
20. R. K. Hanson, "Applications of quantitative laser sensors to kinetics, propulsion and practical energy systems," Proc. Combust. Inst. **33**, 1–40 (2011).
21. Z. Liu, J. F. Barlow, P. Chan, J. C. H. Fung, Y. Li, C. Ren, H. W. L. Mak, and E. Ng, "A review of progress and applications of pulsed Doppler wind LiDARs," Remote Sens. **11**, 2522 (2019).
22. J. Brunker and P. Beard, "Acoustic resolution photoacoustic Doppler velocimetry in blood-mimicking fluids," Sci. Rep. **6**, 20902 (2016).
23. A. Ehn, J. Zhu, X. Li, and J. Kiefer, "Advanced laser-based techniques for gas-phase diagnostics in combustion and aerospace engineering," Appl. Spectrosc. **71**, 341–366 (2017).
24. B. F. Bathel, C. Johansen, J. A. Inman, S. B. Jones, and P. M. Danehy, "Review of fluorescence-based velocimetry techniques to study high-speed compressible flows," in *51th AIAA Aerospace Science Meeting including the New Horizons Forum and Aerospace Exposition* (2013), paper 339.
25. S. Dai, T. Jiang, H. Wu, Z. Zhang, L. Wu, H. Gong, W. Weng, J. Deng, H. Zheng, and W. Lin, "Tunable narrow-linewidth 226 nm laser for hypersonic flow velocimetry," Opt. Lett. **45**, 2291–2294 (2020).
26. I. Ribet, T. Pot, and M. Lefebvre, "Coherent anti-Stokes Raman scattering velocimetry with nearly degenerate pumps," Appl. Phys. B **74**, 445–452 (2002).
27. B. Scherrer, A. Godard, I. Ribet, P. Bouchardy, T. Pot, and M. Lefebvre, "Comparison of dephasing times for vibrational and rotational coherent anti-Stokes Raman scattering: implications for velocimetry," Appl. Phys. B **71**, 859–864 (2000).
28. M. Shangguan, H. Xia, C. Wang, J. Qiu, S. Lin, X. Dou, Q. Zhang, and J. Pan, "Dual-frequency Doppler lidar for wind detection with a superconducting nanowire single-photon detector," Opt. Lett. **42**, 3541–3544 (2017).
29. L. Lombard, M. Valla, C. Planchat, D. Goular, B. Augère, P. Bourdon, and G. Canat, "Eyesafe coherent detection wind lidar based on a beam-combined pulsed laser source," Opt. Lett. **40**, 1030–1033 (2015).
30. F. Li, X. Yu, H. Gu, Z. Li, Y. Zhao, L. Ma, L. Chen, and X. Chang, "Simultaneous measurements of multiple flow parameters for scramjet characterization using tunable diode-laser sensors," Appl. Opt. **50**, 6697–6707 (2011).
31. G. B. Rieker, H. Li, X. Liu, J. B. Jeffries, R. K. Hanson, M. G. Allen, S. D. Wehe, P. A. Mulhall, and H. S. Kindle, "A diode laser sensor for rapid, sensitive measurements of gas temperature and water vapour concentration at high temperatures and pressures," Meas. Sci. Technol. **18**, 1195–1204 (2007).
32. L. S. Chang, J. B. Jeffries, and R. K. Hanson, "Mass flux sensing via tunable diode laser absorption of water vapor," AIAA J. **48**, 2687–2693 (2010).
33. C. L. Strand and R. K. Hanson, "Thermometry and velocimetry in supersonic flows via scanned wavelength-modulation absorption spectroscopy," in *47th AIAA/ASME/SAE/ASEE Joint Propulsion Conference and Exhibit* (2011), p. 5600.
34. I. A. Schultz, C. S. Goldenstein, J. B. Jeffries, and R. K. Hanson, "Spatially-resolved TDLAS measurements of temperature, H_2O column density, and velocity in a direct-connect scramjet combustor," in *52nd Aerospace Sciences Meeting* (2014), paper 1241.
35. K. H. Lyle, J. B. Jeffries, and R. K. Hanson, "Diode-laser sensor for air-mass flux 1: design and wind tunnel validation," AIAA J. **45**, 2204–2212 (2007).
36. F. Adler, P. Masłowski, A. Foltynowicz, K. C. Cossel, T. C. Briles, I. Hartl, and J. Ye, "Mid-infrared Fourier transform spectroscopy with a broadband frequency comb," Opt. Express **18**, 21861–21872 (2010).
37. A. Karpf and G. N. Rao, "Enhanced sensitivity for the detection of trace gases using multiple line integrated absorption spectroscopy," Appl. Opt. **48**, 5061–5066 (2009).
38. A. V. Muraviev, V. O. Smolski, Z. E. Loparo, and K. L. Vodopyanov, "Massively parallel sensing of trace molecules and their isotopologues with broadband subharmonic mid-infrared frequency combs," Nat. Photonics **12**, 209–214 (2018).
39. A. J. Fleisher, B. J. Bjork, T. Q. Bui, K. C. Cossel, M. Okumura, and J. Ye, "Mid-infrared time-resolved frequency comb spectroscopy of transient free radicals," J. Phys. Chem. Lett. **5**, 2241–2246 (2014).
40. D. Luo, Y. Liu, C. Gu, C. Wang, Z. Zhu, W. Zhang, Z. Deng, L. Zhou, W. Li, and H. Zeng, "High-power Yb-fiber comb based on pre-chirped-management self-similar amplification," Appl. Phys. Lett. **112**, 061106 (2018).
41. A. M. Zolot, F. R. Giorgetta, E. Baumann, J. W. Nicholson, W. C. Swann, I. Coddington, and N. R. Newbury, "Direct-comb molecular spectroscopy with accurate, resolved comb teeth over 43 THz," Opt. Lett. **37**, 638–640 (2012).
42. C. Gu, Z. Zuo, D. Luo, Z. Deng, Y. Liu, M. Hu, and W. Li, "Passive coherent dual-comb spectroscopy based on optical-optical modulation with free running lasers," PhotoniX **1**, 7 (2020).
43. G. B. Rieker, F. R. Giorgetta, W. C. Swann, J. Kofler, A. M. Zolot, L. C. Sinclair, E. Baumann, C. Cromer, G. Petron, C. Sweeney, P. P. Tans, I. Coddington, and N. R. Newbury, "Frequency-comb-based remote sensing of greenhouse gases over kilometer air paths," Optica **1**, 290–298 (2014).
44. D. R. Carlson, D. D. Hickstein, A. Lind, S. Droste, D. Westly, N. Nader, I. Coddington, N. R. Newbury, K. Srinivasan, S. A. Diddams, and S. B. Papp, "Self-referenced frequency combs using high-efficiency silicon-nitride waveguides," Opt. Lett. **42**, 2314–2317 (2017).
45. M. Yan, W. Li, K. Yang, H. Zhou, X. Shen, Q. Zhou, Q. Ru, D. Bai, and H. Zeng, "High-power Yb-fiber comb with feed-forward control of nonlinear-polarization-rotation mode-locking and large-mode-area fiber amplification," Opt. Lett. **37**, 1511–1513 (2012).
46. A. C. Chan, E. Y. Lam, and V. J. Srinivasan, "Comparison of Kasai autocorrelation and maximum likelihood estimators for Doppler optical

coherence tomography," IEEE Trans. Med. Imag. **32**, 1033–1042 (2013).
47. F. Cappelli, G. Campo, I. Galli, and P. Natale, "Frequency stability characterization of a quantum cascade laser frequency comb," Laser Photon. Rev. **10**, 623–630 (2016).
48. C. J. Sansonetti, C. E. Simien, J. D. Gillaspy, J. N. Tan, S. M. Brewer, R. C. Brown, S. Wu, and J. V. Porto, "Absolute transition frequencies and quantum interference in a frequency comb based measurement of the ^{6,7}Li lines," Phys. Rev. Lett. **107**, 023001 (2011).
49. B. C. Smith, B. Lomsadze, and S. T. Cundiff, "Optimum repetition rates for dual-comb spectroscopy," Opt. Express **26**, 12049–12056 (2018).
50. E. Baumann, F. R. Giorgetta, W. C. Swann, A. M. Zolot, I. Coddington, and N. R. Newbury, "Spectroscopy of the methane ν_3 band with an accurate midinfrared coherent dual-comb spectrometer," Phys. Rev. A **84**, 062513 (2011).
51. J. Li, B. Yu, W. Zhao, and W. Chen, "A review of signal enhancement and noise reduction techniques for tunable diode laser absorption spectroscopy," Appl. Spectros. Rev. **49**, 666–691 (2014).
52. Z. Chen, M. Yan, T. W. Hänsch, and N. Picqué, "A phase-stable dual-comb interferometer," Nat. Commun. **9**, 3035 (2018).
53. N. R. Newbury, I. Coddington, and W. Swann, "Sensitivity of coherent dual-comb spectroscopy," Opt. Express **18**, 7929–7945 (2010).
54. M. Yan, P. Luo, K. Iwakuni, G. Millot, T. W. Hänsch, and N. Picqué, "Mid-infrared dual-comb spectroscopy with electro-optic modulators," Light: Sci. Appl. **6**, e17076 (2017).
55. Z. Chen, T. W. Hänsch, and N. Picqué, "Mid-infrared feed-forward dual-comb spectroscopy," Proc. Natl. Acad. Sci. USA **116**, 3454–3459 (2019).
56. G. Ycas, F. R. Giorgetta, E. Baumann, I. Coddington, D. Herman, S. A. Diddams, and N. R. Newbury, "High-coherence mid-infrared dual-comb spectroscopy spanning 2.6 to 5.2 μm," Nat. Photonics **12**, 202–208 (2018).
57. H. Timmers, A. Kowligy, A. Lind, F. C. Cruz, N. Nader, M. Silfies, G. Ycas, T. K. Allison, P. G. Schunemann, S. B. Papp, and S. A. Diddams, "Molecular fingerprinting with bright, broadband infrared frequency combs," Optica **5**, 727–732 (2018).